

Supporting information for:

Design and synthesis of a push-pull arylene–vinylene terpyridyl conjugate: multifunctional behaviors exhibited by a single molecule

Amit Sil,^a Utsav Ghosh,^a Suman Dolai,^a Soumitra Manna,^a Apurba Maity^a and Sanjib K. Patra^{*a}

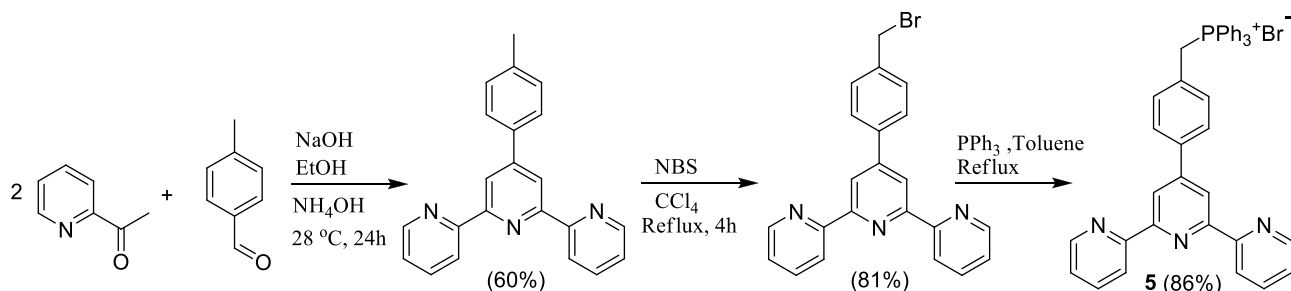
^a*Department of Chemistry, Indian Institute of Technology Kharagpur, Kharagpur-721302, WB, INDIA, E-mail: skpatra@chem.iitkgp.ac.in; Tel: +913222283338*

1.	Synthesis and Characterization	S2-S12
1a.	Syntheses	S2-S3
1b.	Materials and methods	S3-S4
1c.	NMR spectra	S4-S8
1d.	FTIR spectra	S9
1e.	Mass spectrometry	S9-S10
1f.	CHN analysis	S11
1g.	HPLC analysis	S11
1h.	PXRD analysis	S-12
2.	Photophysical properties	S12-S14
2a.	Determination of quantum yield	S12
2b.	Absorption and emission data (solution and solid state)	S13
2c.	Concentration dependent PL study	S13-S14
3.	Detection of NACs	S14-S19
3a.	Visual appearance of probe in absence and presence of NACs	S14
3b.	Fluorescence titration studies of probe towards nitroaromatics	S15
3c.	Absorption and emission spectral overlap of the probe	S15
3d.	Calculation of Stern-Volmer constant	S16
3e.	Calculation of limit of detection (LOD)	S16-S17
3f.	Time resolved fluorescence data and Lifetime measurement	S17
3g.	PL response (as thin film sample) of probe towards picric acid (PA) vapour	S18-S19
3h.	Changes in emission spectra of the probe (as thin film) towards PA solution	S19
3i.	Contact mode detection of picric acid	S19
4.	FESEM analysis	S20
5.	Detection of Hg ²⁺	S21-S24
5a.	Absorption and Emission spectra in 1:1 THF:H ₂ O	S21
5b.	Absorption and Emission spectra towards different metal ions	S21
5c.	Visual appearance towards different metal ions	S22
5d.	Absorption titration study towards Hg ²⁺	S22
5e.	Emission spectral titration profile towards Hg ²⁺ for stoichiometric determination	S23
5f.	Determination of binding constant and LOD of probe for sensing Hg ²⁺	S23-S24
5g.	Reversibility studies of the probe in detection of Hg ²⁺	S24
6.	Theoretical studies	S24-S28
7.	References	S28-S29

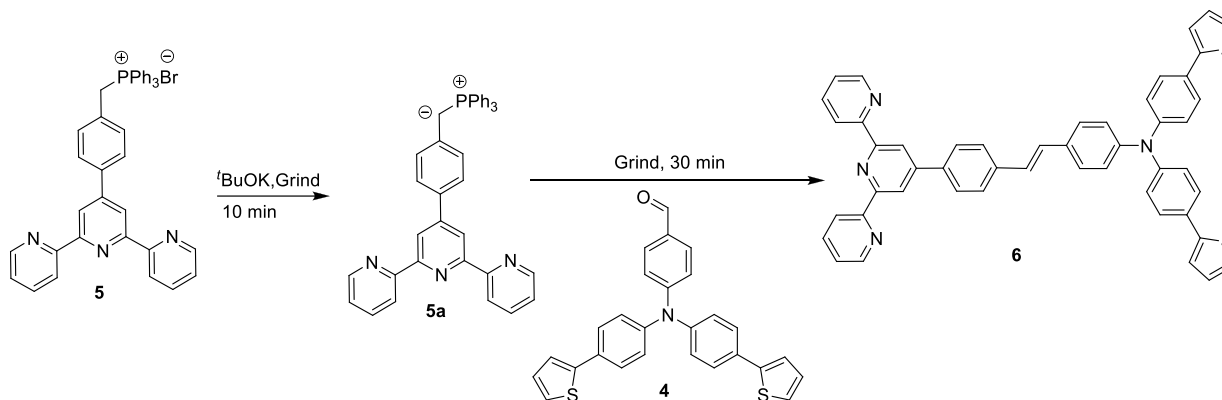
1. Synthesis and Characterization

1a. Synthesis

Compounds **1-3** and **5** have been synthesized following the literature procedure.^{S1}



Scheme S1. Synthetic route of compound **5** (Yield in the parenthesis).



Scheme S2. Schematic representation of the synthesis of compound **6** (Top: Visual colour change).

Synthesis of compound **4**-(bis(4-bromophenyl)amino)benzaldehyde (**3**)

In an oven dried Schlenk flask thoroughly purged with Ar, NBS (1 g, 5.64 mmol) was added to a solution of 4-(diphenylamino)benzaldehyde (0.769 g, 2.82 mmol) in anhydrous THF (20 mL), then the mixture was stirred at 0°C for 12 h. After solvents were evaporated, the residue was further purified by silica gel chromatography with ethylacetate/ hexanes (5:95 vol/vol) as the eluent to afford **3** as a yellow solid (Yield: 1 g, 82%). ¹H NMR (400 MHz,) δ 9.84 (s, 1H, -CHO), 7.71 (d,

$J = 8.4$ Hz, 2H), 7.45 (d, $J = 8.4$ Hz, 4H), 7.03 (t, $J = 8.6$ Hz, 6H); ^{13}C NMR (101 MHz, CDCl_3) δ 190.6 (-CHO), 152.6, 145.3, 133.2, 131.6, 130.4, 127.6, 120.7, 118.3; LCMS (ESI+): m/z $[\text{M}+\text{H}]^+$ calcd for: $\text{C}_{19}\text{H}_{14}\text{Br}_2\text{NO}$: 429.943; found: 429.912.

Synthesis of 4-(2,2':6',2''-terpyridyl-4')-benzyl triphenylphosphonium bromide (5)

A mixture of **2** (6.0 g, 18 mmol) and triphenylphosphine (5.89 g, 22.4 mmol) in anhydrous toluene (120 mL) was heated to reflux for 12h. The solution was then allowed to cool to room temperature and off-white precipitate from the resulting solution was filtered off and washed with toluene to remove the excess PPh_3 . The product was recrystallized from anhydrous ethanol to give white solid product **5** (9.7 gm, 86%). ^1H NMR (CDCl_3 , 400 MHz): δ 5.62 (d, $J = 16$ Hz, 2H, methylene), 7.14 – 7.25 (m, 3H), 7.27 – 7.30 (m, 2H), 7.57(d, $J = 8\text{Hz}$, 2H), 7.61 – 7.66 (m, 6H), 7.74 – 7.83 (m, 10H), 8.50 (s, 2H, py), 8.55 (d, $J = 8\text{Hz}$, 2H, py), 8.64 (d, $J = 4\text{Hz}$, 2H, py) ; $^{13}\text{C}\{^1\text{H}\}$ NMR (CDCl_3 , 100 MHz): δ 30.7 (methylene), 117.6, 118.4, 118.6, 118.8, 121.6, 124.1, 127.7, 128.4, 129.3, 130.3, 132.4, 136.7, 135.2, 137.1, 138.5, 149.2, 156.1; $^{31}\text{P}\{^1\text{H}\}$ (CDCl_3 , 162 MHz): 23.7 ppm.

1b. Materials and methods.

All moisture sensitive reactions and manipulations were carried out under an atmosphere of pre-purified Ar by using standard Schlenk techniques. The glasswares were oven-dried (at 180°C) and cooled under vacuum. Toluene was dried over Na/benzophenone whereas dry methanol and CCl_4 were obtained by distillation over CaH_2 . Unless otherwise mentioned all chemicals were of analytical grade, obtained from Aldrich, and used without further purification. Triphenylphosphine (PPh_3) and Triphenylamine were purchased from Spectrochem. Silica gel (60–120 mesh) used for column chromatography, was purchased from Merck. 2,2'-Azobisisobutyronitrile (AIBN) and PPh_3 were recrystallized from distilled ethanol. Eluting systems for column chromatography purifications were determined by thin layer chromatography (TLC) analysis. TLC plates were visualized under UV light (254 nm / 365nm). Solvents were evaporated under reduced pressure using a rotary evaporator.

^1H (400 MHz), $^{13}\text{C}\{^1\text{H}\}$ (100 MHz), $^{19}\text{F}\{^1\text{H}\}$ (376 MHz) and $^{31}\text{P}\{^1\text{H}\}$ (162 MHz) NMR spectra were obtained from Bruker Lambda spectrometer using CDCl_3 unless otherwise mentioned. Spectra were internally referenced to residual solvent peaks ($\delta = 7.26$ ppm for proton and $\delta = 77.23$ for carbon (middle peak)) in CDCl_3 . All the coupling constants (J) are given in Hz.

The HRMS mass spectrometry was recorded in ESI⁺ mode (70 eV) in Waters (Model: Xevo-G2QTOF). The absorption and fluorescence spectra were collected using a Shimadzu (Model UV-2450) spectrophotometer and a Hitachi (Model F-7000) spectrofluorimeter respectively. The time-resolved emission decays were recorded using a time correlated single photon counting (TCSPC) picoseconds spectrophotometer (Model IBH, UK). FTIR spectroscopy was recorded in Spectrum-BX (Perkin Elmer). Spin-Coating was performed in SpinNXG-P1 (Apex). FESEM data was recorded in Supra 40, Carl Zeiss microscope.

1c. NMR Spectra

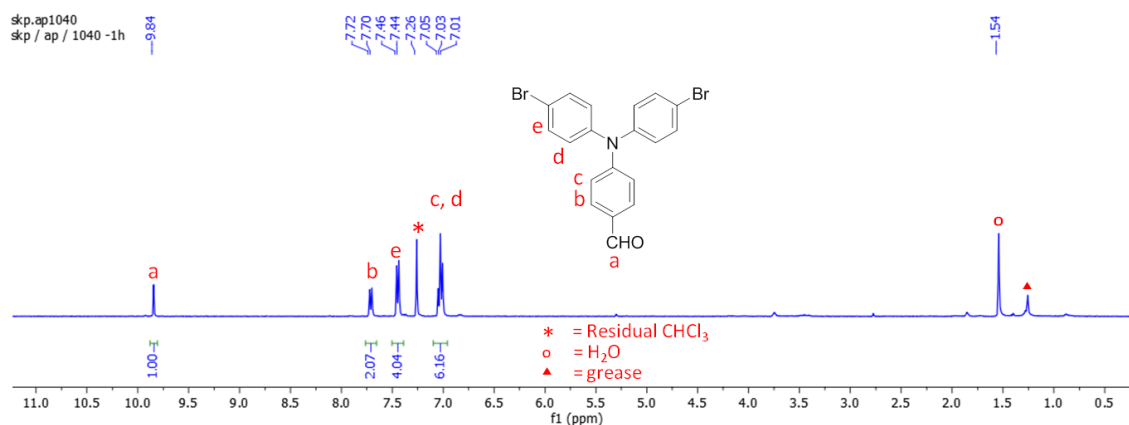


Fig. S1a: ¹H NMR (400 MHz, CDCl₃) spectrum of **3**.

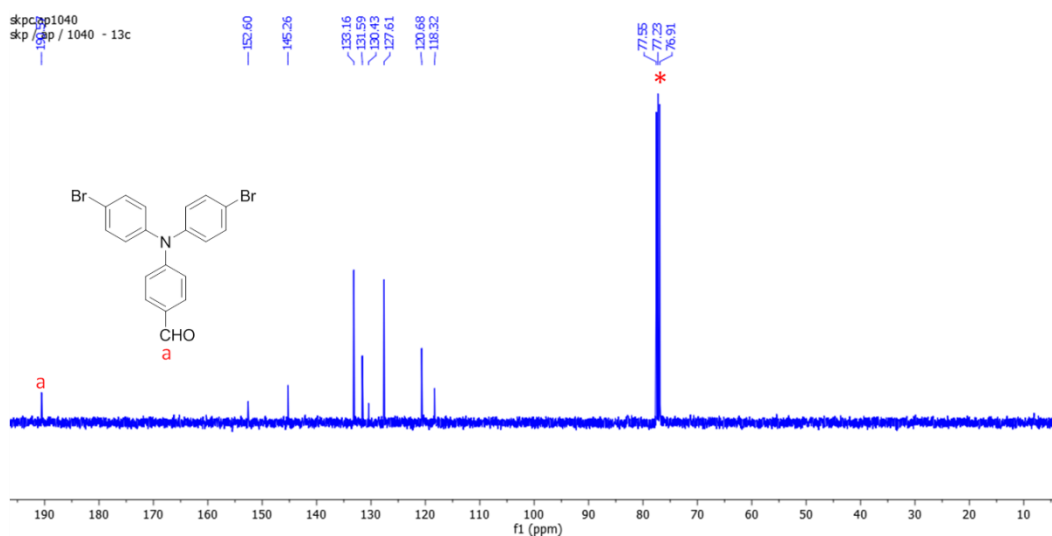


Fig. S1b: ¹³C{¹H} NMR (100 MHz, CDCl₃) spectrum of **3**.

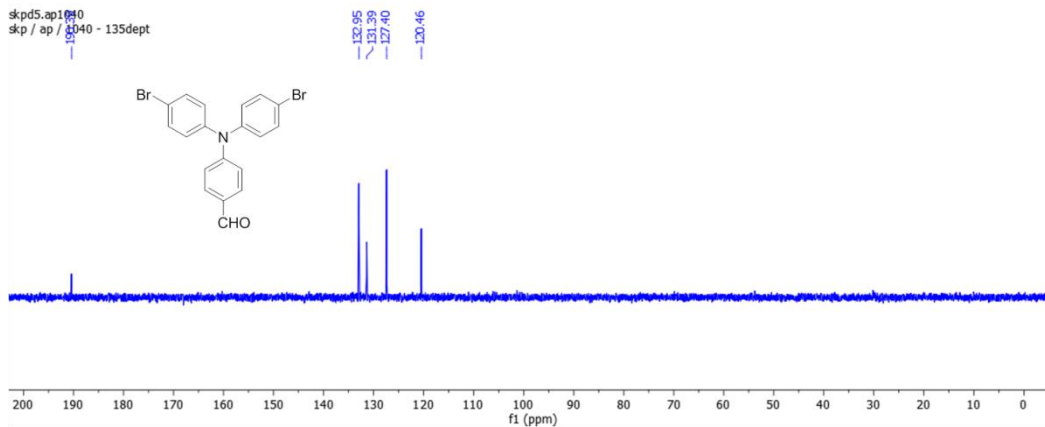


Fig. S1c: DEPT-135 NMR (100 MHz, CDCl_3) spectrum of **3**.

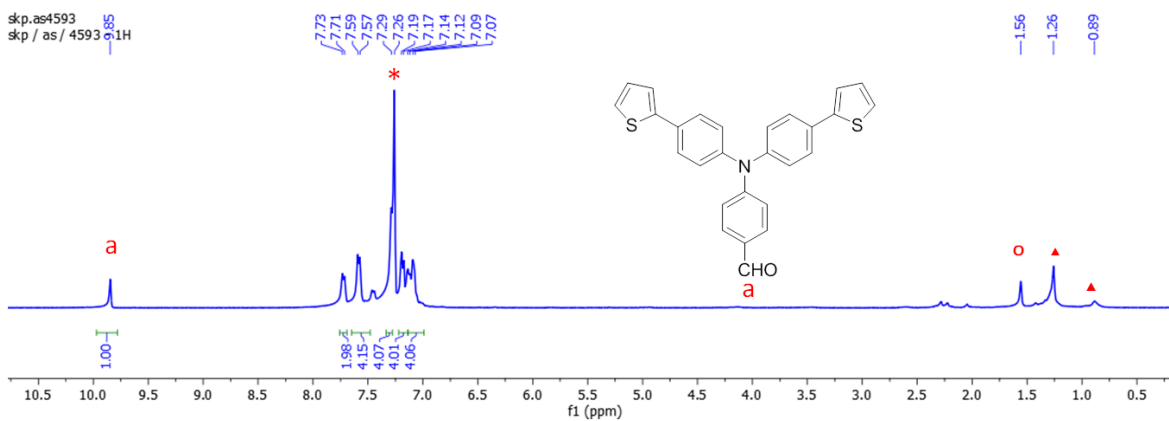


Fig. S2a: ^1H NMR (400MHz, CDCl_3) spectrum of **4**.

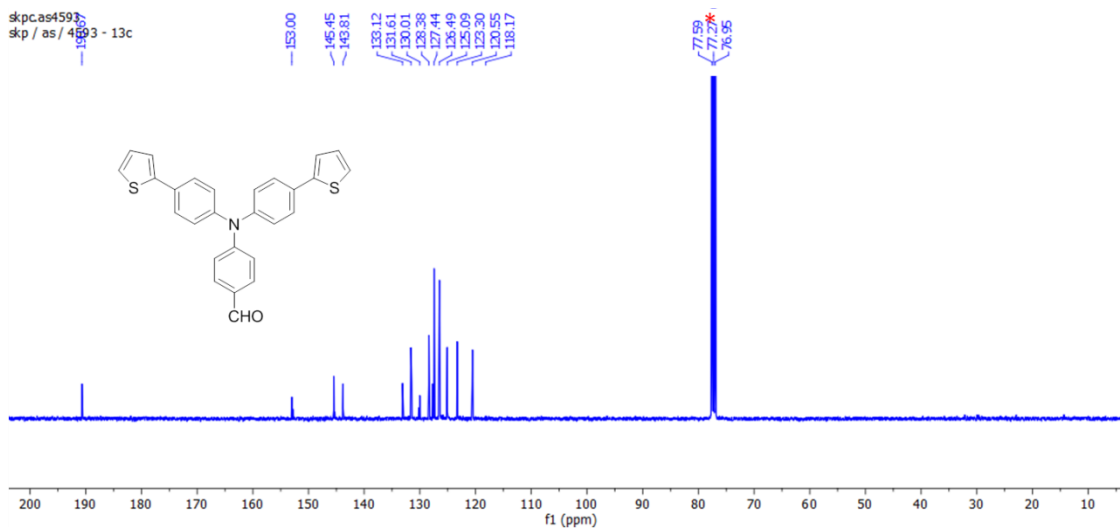


Fig. S2b: $^{13}\text{C}\{^1\text{H}\}$ NMR (100 MHz, CDCl_3) spectrum of **4**.

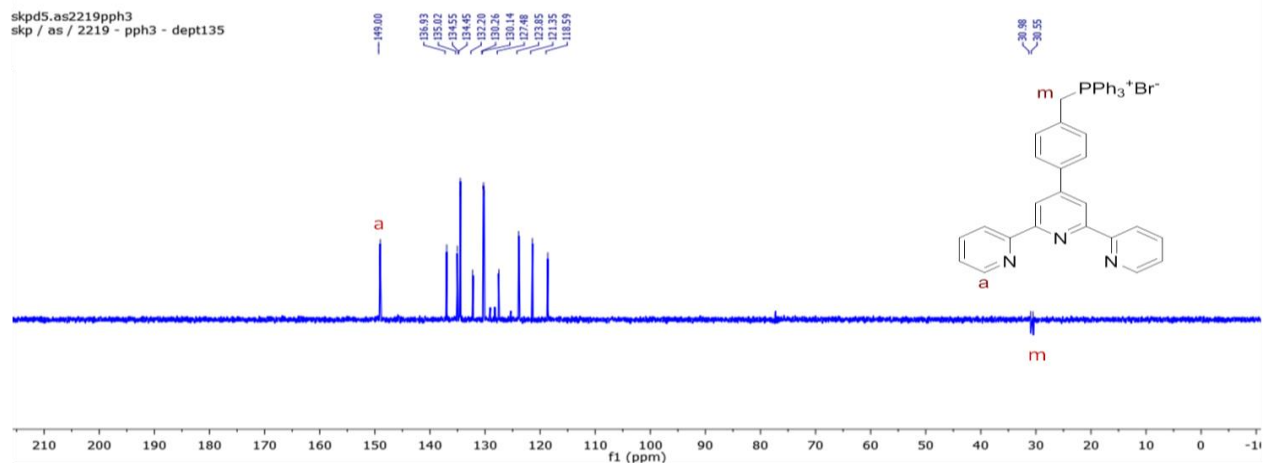


Fig. S3c: DEPT-135 NMR (100 MHz, CDCl_3) spectrum of **5**

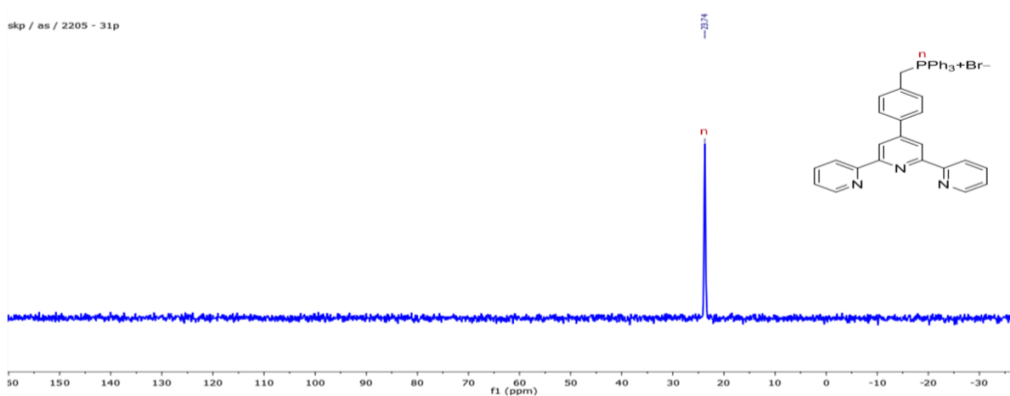


Fig. S3d: $^{31}\text{P}\{^1\text{H}\}$ NMR (CDCl_3 , 162 MHz) spectrum of **5**

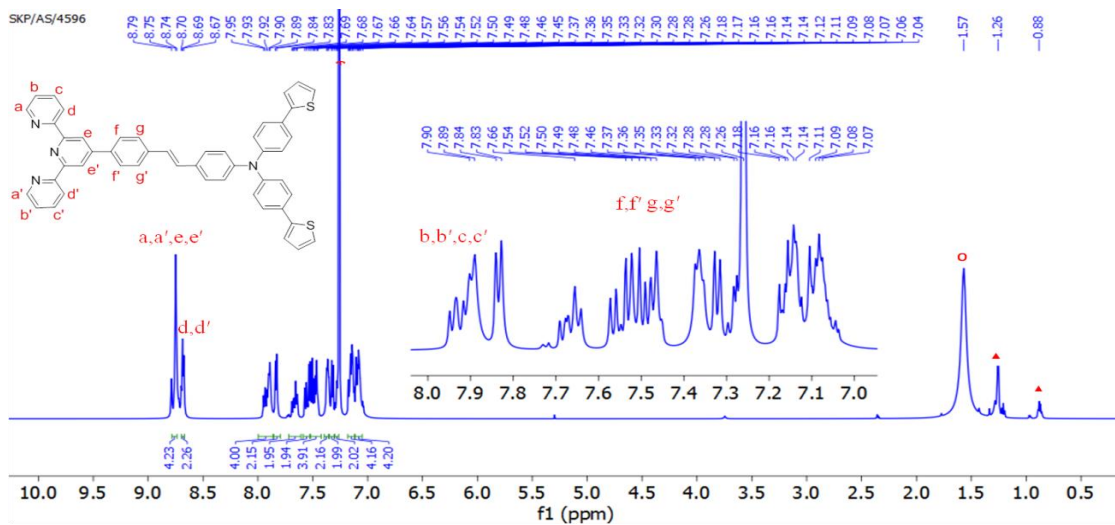


Fig. S4a: ^1H NMR (600 MHz, CDCl_3) spectrum of **6**; the vinyl protons are overlapped with residual CHCl_3 protons and the unassigned aromatic protons assigns the arylene group protons.

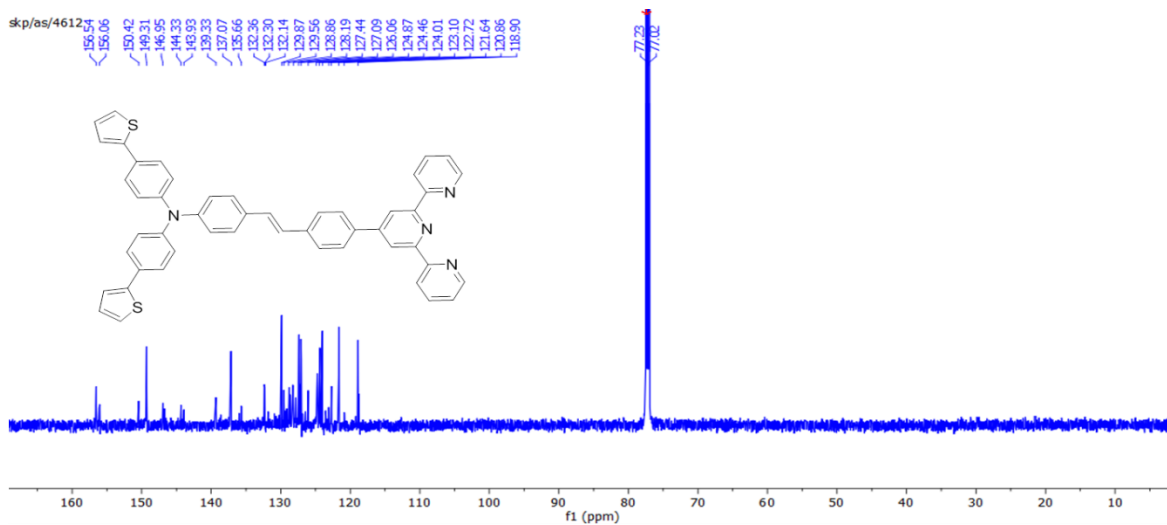


Fig. S4b: $^{13}\text{C}\{^1\text{H}\}$ NMR (150 MHz, CDCl_3) spectrum of **6**.

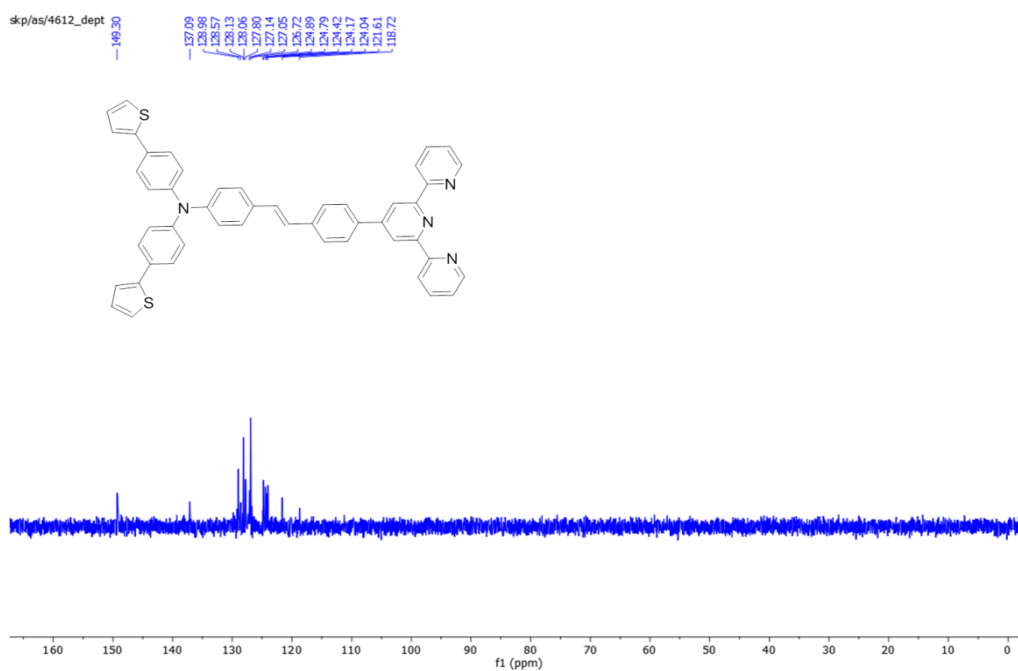


Fig. S4c: DEPT-135 NMR (150 MHz, CDCl_3) spectrum of **6**.

1d. FTIR Spectra (measured as KBr pellets)

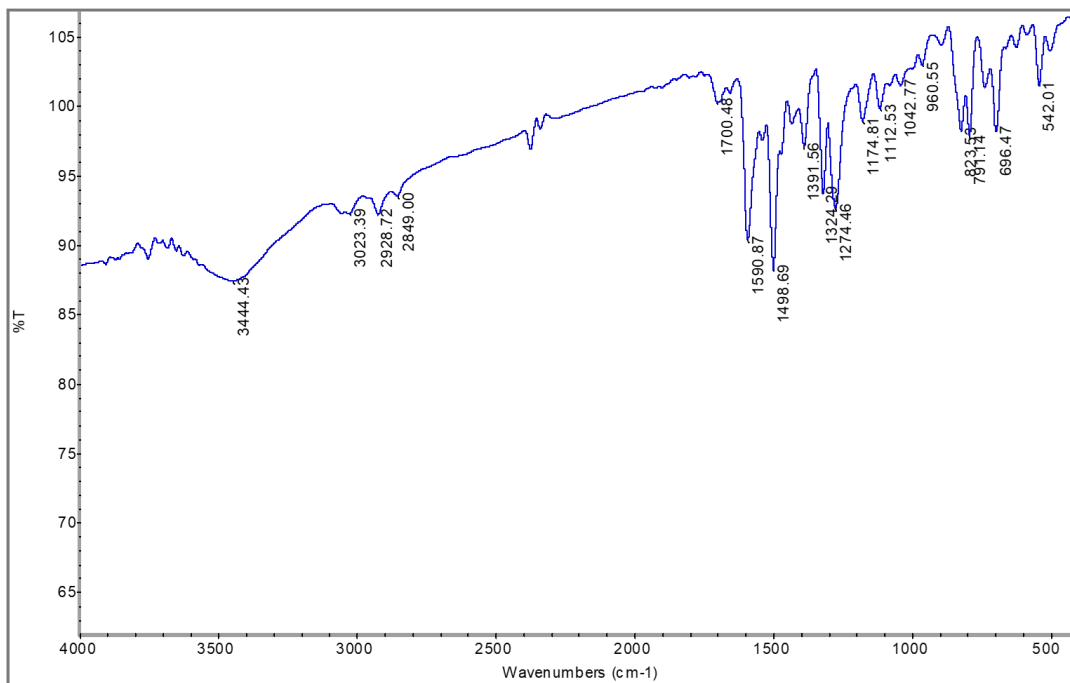


Fig. S5: FTIR spectrum of **6**

1e. Mass spectrometry

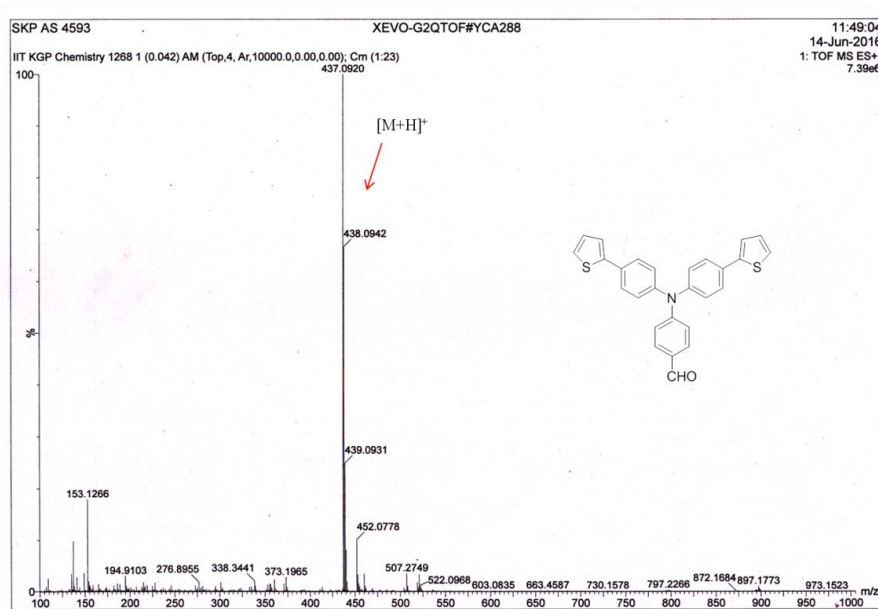


Fig. S6: HRMS (ESI⁺) of **4**

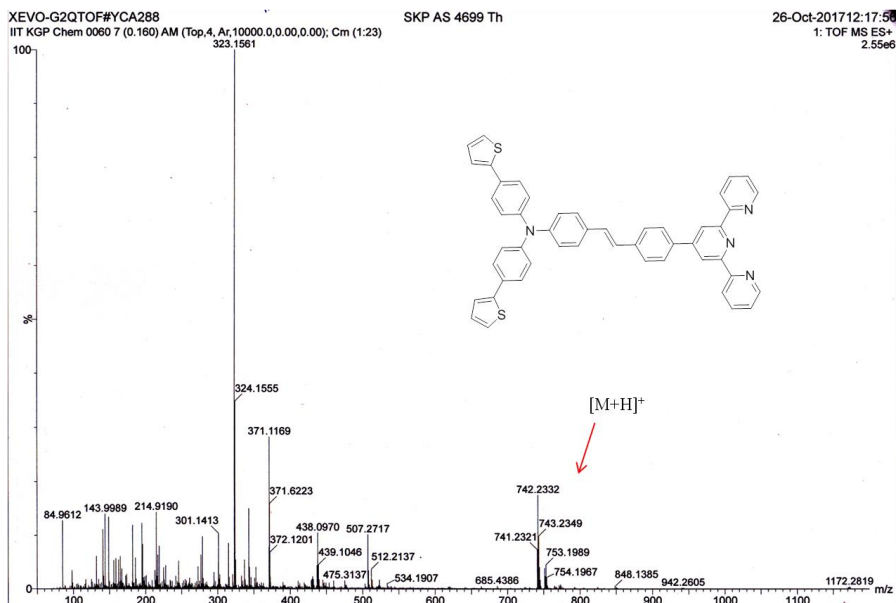


Fig. S7: HRMS (ESI⁺) of 6

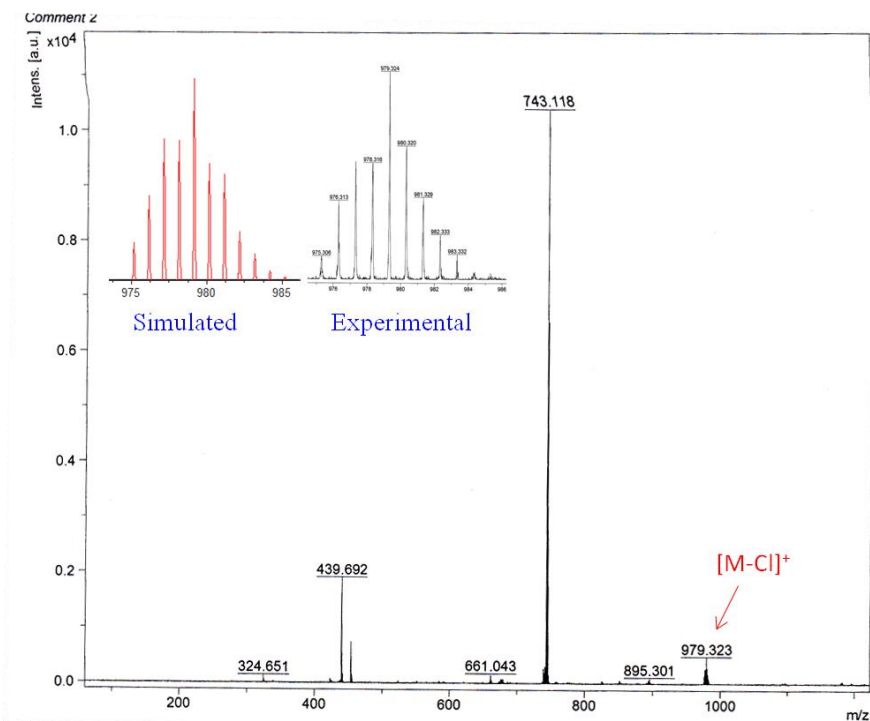


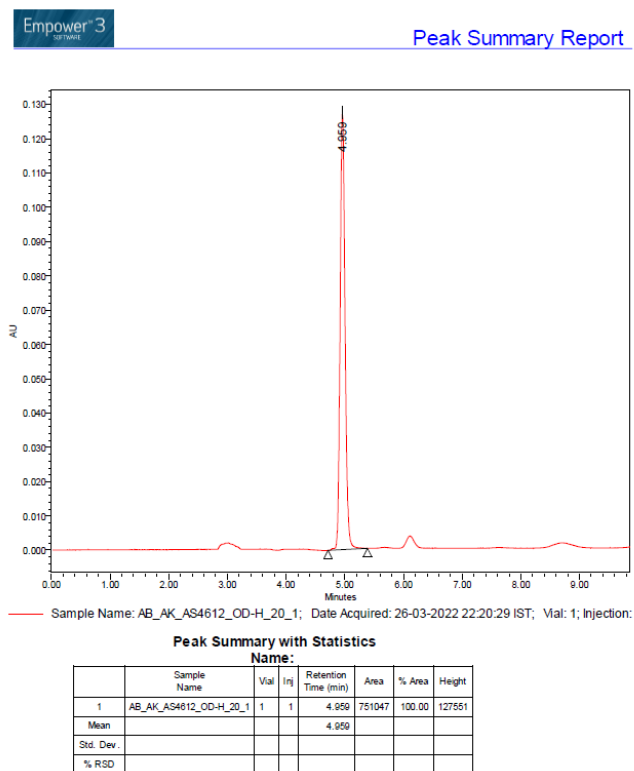
Fig. S8. MALDI-TOF mass spectrometry of and simulated isotopic distribution at the molecular ion peak of 1:1 6-Hg²⁺ complex (Inset: Experimental and simulated isotopic distribution at the molecular ion peak).

1f. CHN analysis of compound 6

<p>Anal. Calc. for $C_{49}H_{34}N_4S_2$: C, 79.21; H 4.61; N, 7.54. Found: C, 77.66; H 4.40; N, 8.06.</p>	<pre> DATE 10 03 22 TIME 17 21 28 P_ID IACS RUN 33 ID 4612 WEIGHT 1.894 SIGNALS ZR 2881 NR 4231 CR 31002 HR 35129 CARBON 77.66% HYDROGEN 4.40% NITROGEN 8.06% BLANKS 13 647 356 KFACTORS 18.192 41.782 6.514 OXFILL COMB BOOST1 BOOST2 1 5 0 0 FILL TIME 25 SECONDS </pre>
--	---

1g. HPLC analysis of compound 6

The purity of the compound was determined by HPLC analysis using a Chiralpak OD-H column.
Solvent: *n*-hexane/2-propanol = 80/20.
Flow rate: 1.0 mL, Detection: at 254 nm.



1h. PXRD analysis

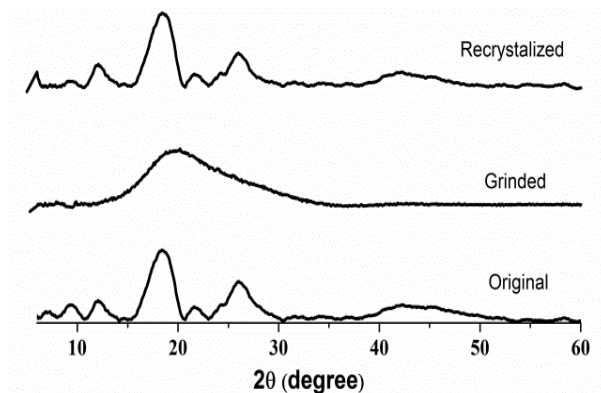


Fig S8: PXRD patterns of **6** in different solid-states: as-synthesized, and during grinding and recrystallized.

2. Photophysical properties

2a. Determination of Quantum yield

All the UV–Vis absorption and emission spectra were recorded using a Shimadzu UV–Vis spectrophotometer (model UV 2450) and a Spex Fluorolog-3 spectrofluorimeter (model FL3–11) respectively. The concentration of the probe was maintained at 10^{-5} M. Fluorescence quantum yields were measured with respect to a secondary standard quinine sulphate ($\lambda_{\text{abs}} = 350$ nm) in 0.1 M H_2SO_4 ($\Phi = 0.54$) at 298 K, following the equation.^{S2}

$$\frac{\Phi_S}{\Phi_R} = \frac{A_S}{A_R} \times \frac{(Abs)_R}{(Abs)_S} \times \frac{\eta_S^2}{\eta_R^2}$$

Here, Φ represents the quantum yield, (Abs) represents the absorbance, A represents the area under the fluorescence curve, and η is the refractive index of the medium. The $\eta_{\text{THF}/\text{H}_2\text{O}}$ was calculated using Arago-biot (AB) equation.^{S3} The subscript S and R denote the corresponding parameters for the sample and reference respectively.

2b. Absorption and emission spectra of **6** in solution and solid state

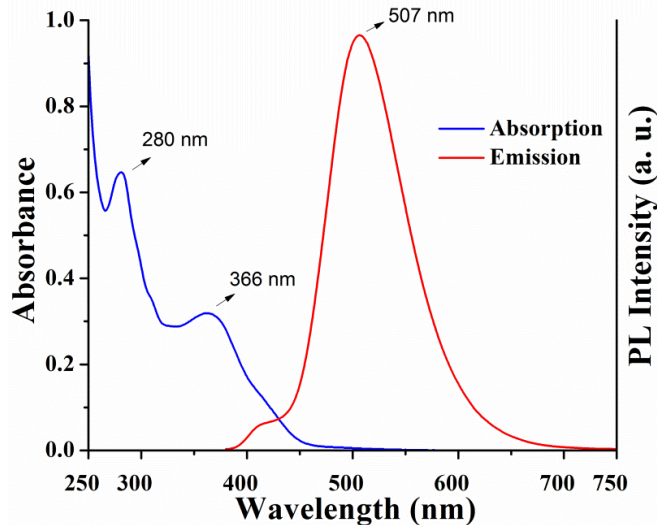


Fig. S9: Absorption and emission spectra of **6** in 1×10^{-5} M CHCl_3 at ambient temperature.

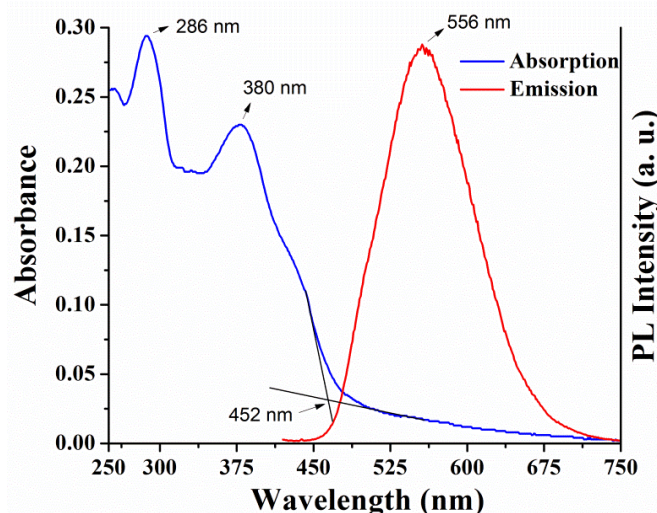


Fig. S10: Solid state absorption and emission spectra of **6** at ambient temperature. The optical energy band gap (E_g^{opt}) of the probes was calculated as 2.74 eV by inspecting the edge of the solid state absorption spectra by using the equation $E_g^{\text{opt}}(\text{eV}) = 1240 / \lambda_{\text{cut off}}$

2c. Concentration dependent fluorescence study

To determine the optimum concentration in which self-aggregation of the sensing probe in solution is less, the concentration dependent emission spectra (1×10^{-3} M to 1×10^{-5} M) was recorded in CHCl_3 . All the arylene-vinylene conjugated terpyridines displayed less aggregation behavior with concentration 10^{-5} M as evidenced from concentration-dependent fluorescence study.

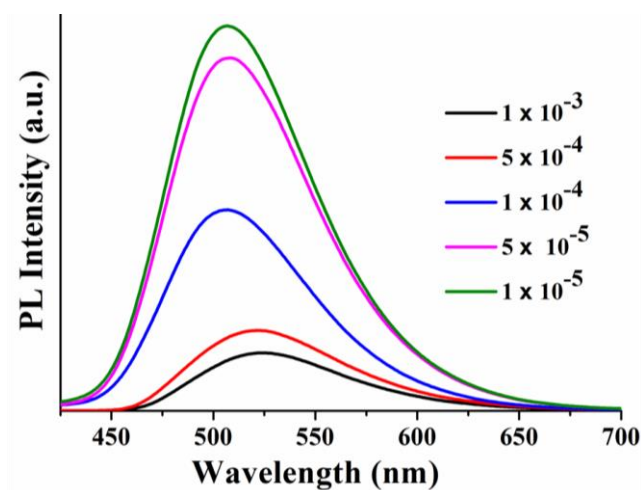


Fig. S11: Concentration dependent fluorescence spectra ($\lambda_{\text{ex}} = 390 \text{ nm}$) of **6** in CHCl_3 at ambient temperature.

3. Detection of NACs

The sensing application was conducted in dilute solution (in the concentration range of ca. 10^{-5} M in CHCl_3) to nullify the self-association behavior and loss of sensitivity. This also minimizes the inner-filter effect. Moreover, the absorption spectra PA does not overlap significantly with the emission spectra of the probe (Figure S14) implying the minimal secondary hetero-inner filter effect. Thus, no fluorescence intensity correction is needed.

3a. Visual appearance of the probes in absence and presence of PA

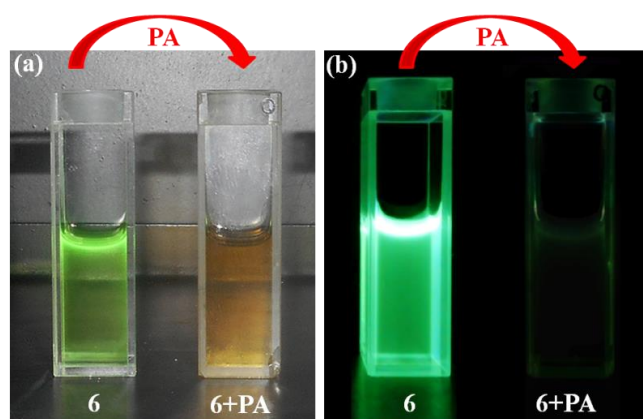


Fig. S12: Visual appearance of **6** before and after the addition of PA (Left) under ambient light, (Right) under UV illumination at 365 nm.

3b. Fluorescence titration studies of the probe towards NACs

The fluorescence spectroscopic titrations were performed with a continuous variation of concentrations ($\sim 1 \times 10^{-5}$ M to $\sim 1 \times 10^{-3}$ M) of NACs in CHCl_3 .

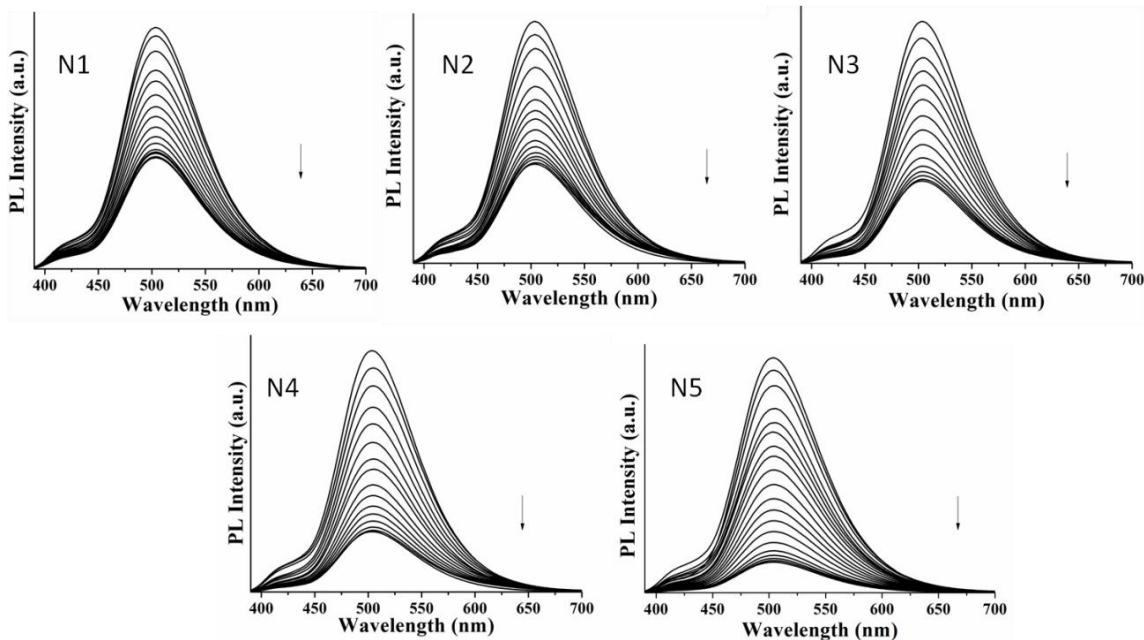


Fig. S13: Fluorescence quenching behaviour of **6** upon incremental addition of different NACs N1: NB, N2: NT, N3: HNB, N4: NBA, N5: DNT.

3c. Spectral overlap between absorption and emission spectra of the probes.

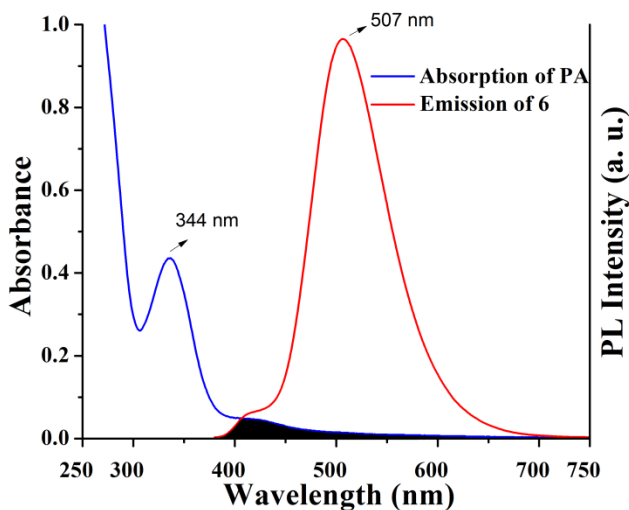


Fig. S14: Absorption spectra of PA and emission spectra of **6** in CHCl_3 (1×10^{-5} M) at ambient temperature.

3d. Calculation of Stern–Volmer constants:

The sensitivity of the sensing probes (**6**) towards the nitroaromatics was estimated from their Stern–Volmer constants, K_{sv} as determined from the equation:

$$I_0/I = 1 + K_{sv} [Q]$$

Where, I_0 and I are the fluorescence intensities in the absence and presence of nitroaromatics respectively, and the Stern–Volmer plots were plotted as a function of the nitroaromatic concentration, $[Q]$. The Stern–Volmer constants, K_{sv} can be calculated from the slope of the Stern–Volmer plots.

Table S1: Association constant (M^{-1}) of the sensing probes toward different NACs

NACs	Association Constant (M^{-1})	NACs	Association Constant (M^{-1})
NB	7.51×10^{-3}	HNB	1.63×10^{-4}
NT	9.81×10^{-3}	DNT	2.04×10^{-4}
NBA	1.35×10^{-4}	PA	2.47×10^{-4}

3e. Calculation of the Limit of Detection (LOD):

The limit of detection (LOD) of the sensing probe (**6**) was determined from emission spectra. I_0 - I values (intensity changes of the emission band centered at 507 nm) were plotted against the concentration (M) of PA (Figure 6a in the manuscript), and LOD was determined using the following equation: $DL = 3\sigma/S$.

Here, σ is the standard deviation of the blank solution; S is the slope of the between fluorescence intensity and picric acid concentration. The value of σ has been estimated from emission spectra of the free polymer sample without nitroaromatic analytes for an appropriate numbers (8 to 10 times). To get the slope (S), change in fluorescence intensity data at λ_{em} of 507 nm was plotted against the concentration of picric acid. Emission spectra was recorded by treating PA solution with varying concentration (*ca.* 10^{-4} M to 10^{-5} M in $CHCl_3$) to the probe of *ca.* 1×10^{-5} M in $CHCl_3$. There was a good linear relationship between fluorescent intensity data and concentrations of PA, indicating quantitative detection.

The important parameters for the LOD calculations of probe **6** (corresponding to Figure 6b in the manuscript) in presence of PA are shown below.

Equation	$y = a + b \cdot x$		
Weight	No Weighting		
Residual Sum of Squares	21185.81542		
Pearson's r	0.99467		
Adj. R-Square	0.98805		
		Value	Standard Error
1	Intercept	55.7669	29.88927
	Slope	7.51899E7	2.75503E6

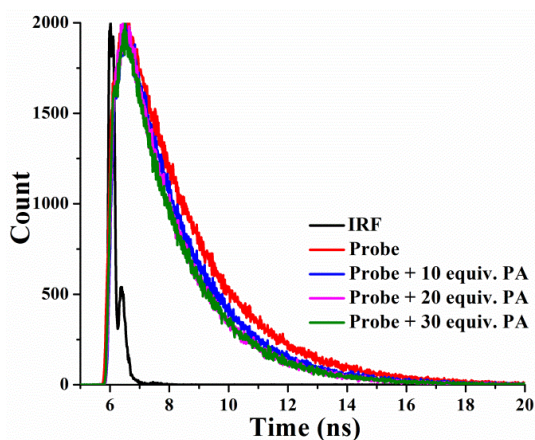
3f. Time resolved fluorescence spectra of the probe, and with PA

The time-resolved emission decays were recorded using a time correlated single photon counting (TCSPC) picoseconds spectrophotometer. Compound **6** was excited using a picoseconds diode laser at 340 nm (IBH, UK, Nanoled). The signals were recorded at magic angle (54.71) using a Hamamatsu micro channel plate photomultiplier tube (3809U). The typical instrument response functions in our setup are 100 ps. Time-resolved fluorescence decays were analyzed using IBH DAS-6 decay analysis software. The radiative and non-radiative decay constants were calculated from the equations, $k_r = \Phi / \tau$ and $k_{nr} = (1 - \Phi) / \tau$, where Φ = quantum yield and τ = lifetime and were tabulated in Table S1.

Table S2: Time resolved fluorescence data of **6** in CHCl_3

<i>Probe</i>	$\langle \tau \rangle^a / \text{ns}$	$k_{nr} (\text{s}^{-1}) / 10^{10}$	$k_r (\text{s}^{-1}) / 10^{10}$
6	2.27	1.58	2.81

^aError limit = $\pm 5\%$



Probe	$\langle \tau \rangle^a / \text{ns}$
6	2.27
6 + 10 equiv. PA	2.085
6 + 20 equiv. PA	1.92
6 + 30 equiv. PA	1.95

Fig. S15: Time resolved fluorescence spectra of **6** in presence and absence of PA.

3g. PL response in solid state (as thin film sample) towards picric acid vapour

The quartz plates (17 x 15 x 1 mm³) were cleaned in a fresh piranha solution (7:3 mixture of 98% H₂SO₄ and 30% H₂O₂), washed with Milli-Q water, and followed by ultrasonication in alkaline isopropanol and 0.1 M aqueous HCl at 60 °C for 1 h each. After 3 careful washing with Milli-Q water, thin film of the sensing probes (6) were prepared by spin coating on quartz plate. A solution of the sensing probe in chloroform (~3 x 10⁻⁴M) was dropped on quartz plate and it was spin coated at 1000 rpm for 60 second followed by 1500 rpm for 120 seconds. PL data of the film was measured. After that the film was dipped in different concentration of aqueous picric acid solution for 10 min followed by repetitive and extensive washing by Milli-Q water to remove any unbound (free) picric acid. After drying in air, PL response was recorded.

For the vapour phase study, the thin film was exposed to the picric acid vapour at room temperature. The PL spectra were recorded with different time interval after exposing the thin film to the picric acid vapour. For the film repeatability measurement the thin film was exposed to picric acid vapour for 300 sec and the emission spectrum was recorded. After the each measurement the film was washed with ethanol: water mixture and dried under hot air and the emission spectra was recorded again and the whole process was repeated again for the repeatability test.

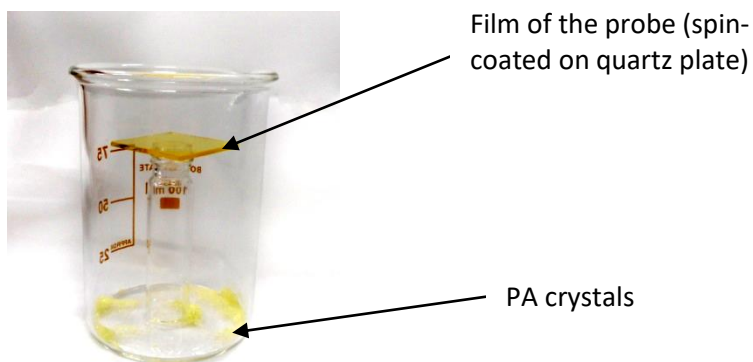


Fig. S16: Experimental set up for demonstrating sensing of PA vapour.

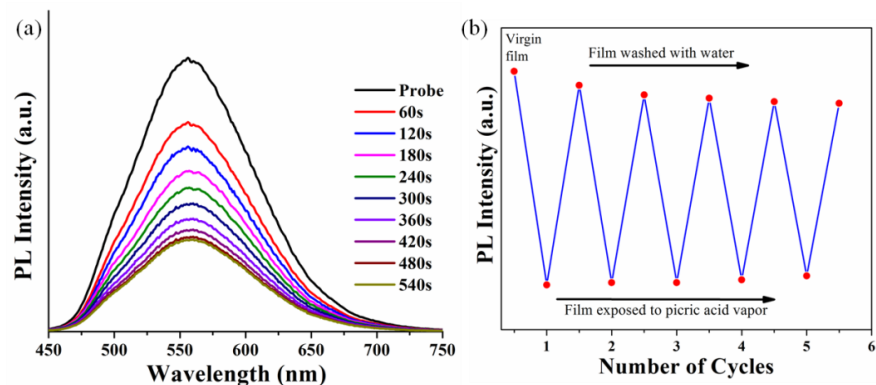


Fig. S17: (a) Quenching of fluorescence intensity of the thin film of **6** upon exposure to PA vapor by varying exposure time; (b) Repeatability test of the probe **6** film demonstrating reusability.

3h. Changes in emission spectra of the probes (as thin film) towards PA solution:

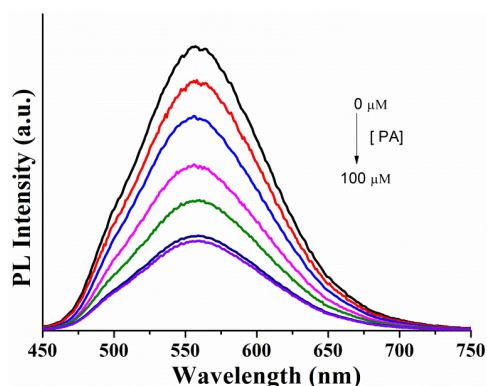


Fig. S18: Emission spectra of **6** (as thin film) after exposing with PA solution by varying the concentrations.

3i. Contact-mode detection

For contact-mode sensing, Whatman-42 filter paper was cut into small pieces and dipped into concentrated DCM solution of the sensing probes and subsequently dried in air. PA solution of different concentration (10^{-3} – 10^{-9} M) were prepared and 10 μL of each solution was drop-casted on each fresh filter paper strip. When the strips were illuminated under UV at 365 nm, dark spots were observed for PA. The spots were prominent for concentrated sample and slowly faded upon dilution which can be detected by naked eye as demonstrated in Figure 10 (in the manuscript).

4. FESEM analysis

Preparation of sample for SEM analysis: The sample for FESEM analysis was prepared on a clean 1 cm × 1.5 cm aluminium plate. A solution of the probe in chloroform ($\sim 5 \times 10^{-4}$ M) was dropped on the alumina substrate, and it was dried under a closed chamber for 2 h. The surface morphology analyses were performed by SEM. The film was dipped in aqueous solution of picric acid for 5 min followed by repetitive and extensive washing by Milli-Q water to remove the unbound (free) picric acid. The surface morphology was again analyzed.

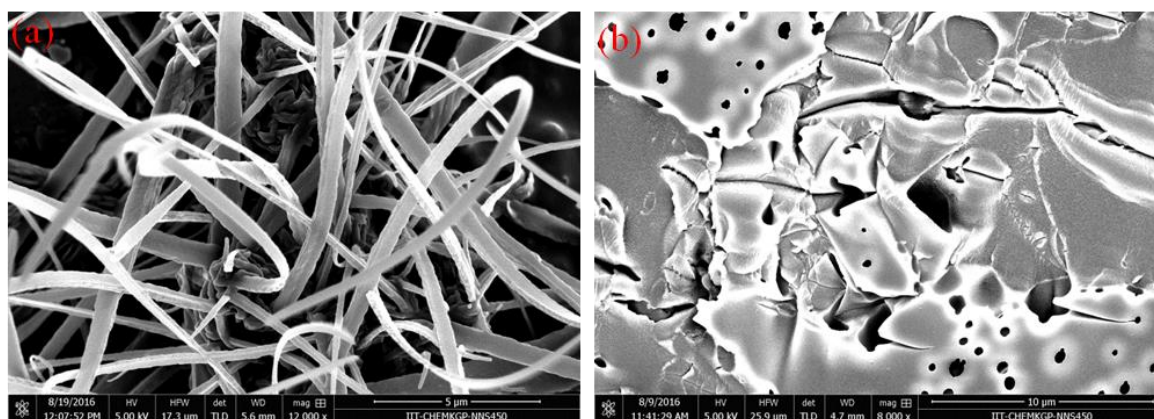


Fig. S19: FESEM images of the sensing **6** (a) before and (b) after treating with PA.

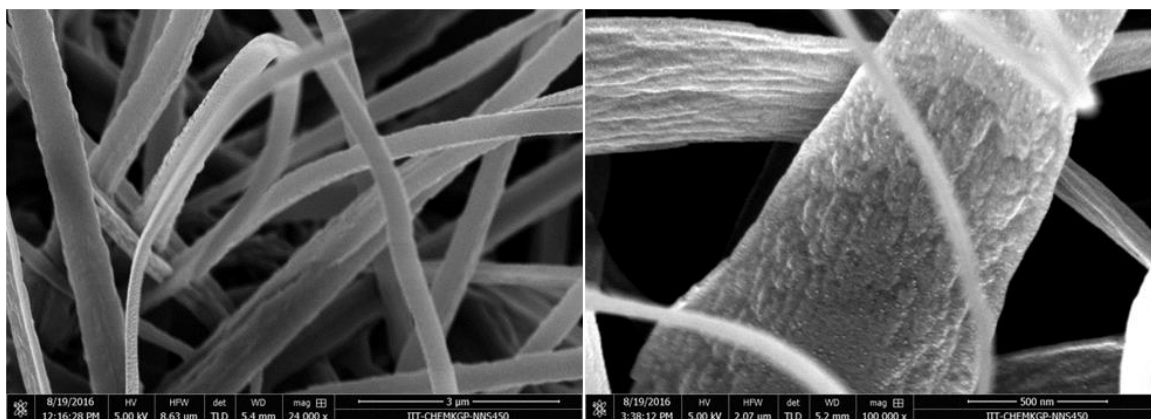


Fig. S20: FESEM images of the sensing probe **6** (Zoomed view).

5. Detection of Hg²⁺ ion

The sensing study was conducted in 5 μ M concentration in 1:1 THF:H₂O.

5a. Absorption and Emission spectra in 1:1 THF:H₂O

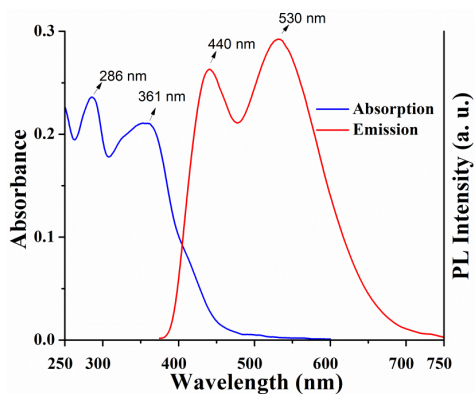


Fig. S21: Absorption and emission spectra of **6** (5 μ M) in 1:1 THF:H₂O.

5b. Absorption and Emission spectra of **6** towards different metal ions

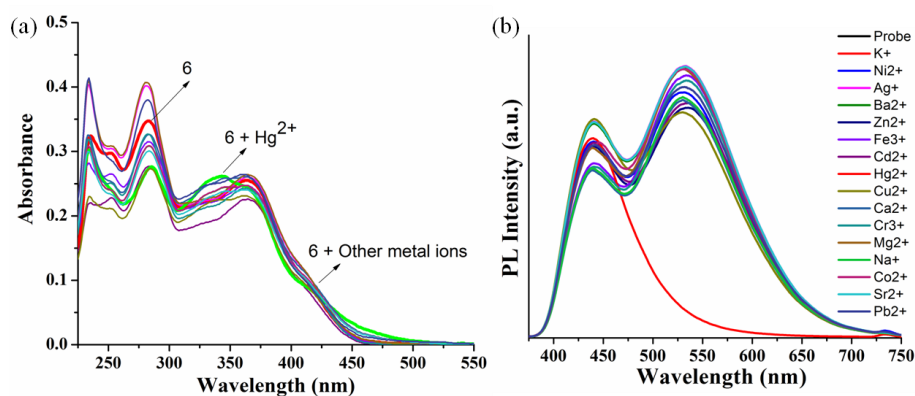


Fig S22: Absorption and Emission spectra of **6** (5 μ M) upon addition of different metal ions (1 eqv.) in THF:H₂O (1:1).

Table S3: Absorption and emission properties of probe **6** before and after addition of Hg²⁺ ion in 1:1 THF:H₂O.

Probe	Absorption	Emission	
	λ_{\max} , nm ($\epsilon \times 10^4$ M ⁻¹ cm ⁻¹)	λ_{em} (λ_{ex}), nm	Φ^a
6	286 (2.3), 361 (2.1)	530, 440 nm (361 nm)	0.24
6-Hg²⁺	290 (2.3), 338 (2.6), 423 (0.68)	440 nm (361 nm)	0.10

^aQuantum yield was determined (in 1:1 THF:H₂O) using quinine sulphate (0.1 M H₂SO₄; $\Phi = 0.54$) as reference.

5c. Visual appearance of the probes in presence of different metal ions

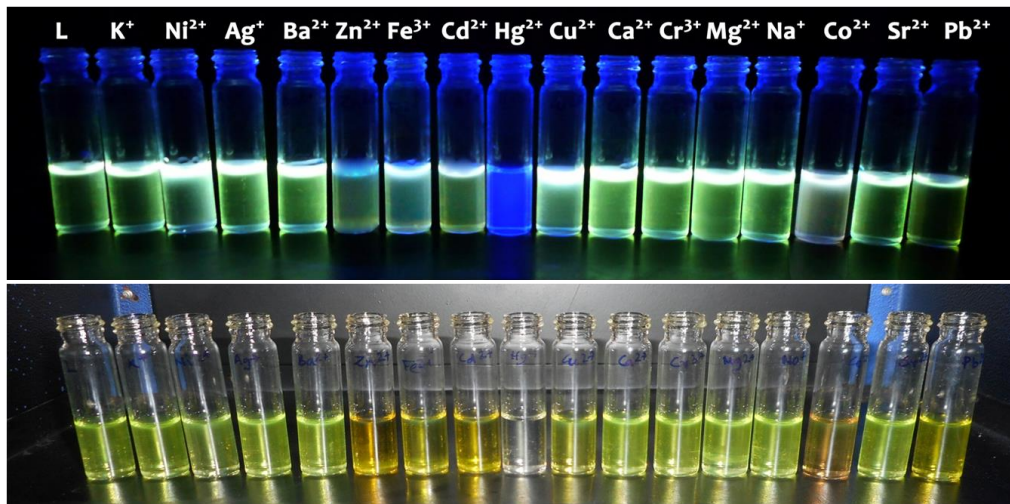


Fig S23: Fluorescence color changes of **6** (2×10^{-4} M in 1:1 THF-H₂O) after addition of different metal ions (1 eqv.) (top) under UV light at 365 nm and (bottom) ambient light.

5d. Absorption titration study

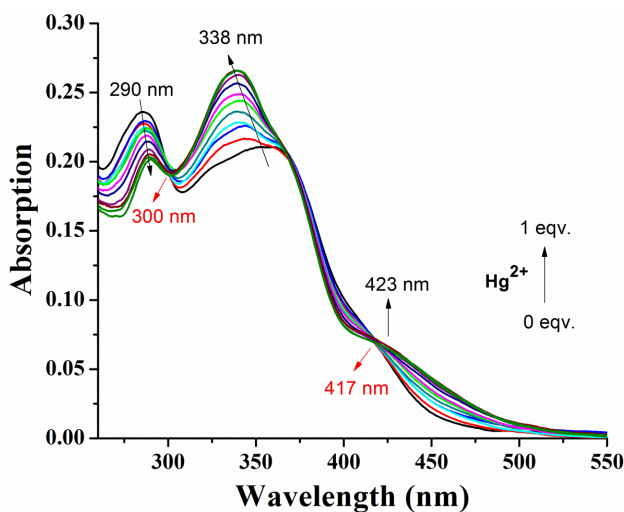


Fig S24: Absorbance spectra of **6** (2 μM) in the presence of increasing equivalent of Hg²⁺ in 1:1 THF-H₂O.

5e. Emission spectral titration profile for stoichiometry determination

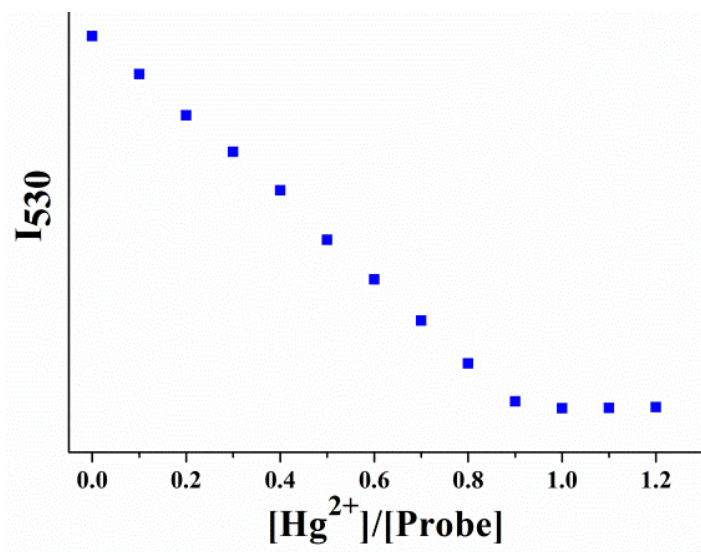


Fig S25: Hg^{2+} titration profile with variation of emission intensity with concentration Hg^{2+} , I_{530} vs $[\text{Hg}^{2+}]/\text{Probe}$, suggesting 1:1 binding stoichiometry.

5f. Determination of binding constant and limit of detection of **6** towards Hg^{2+}

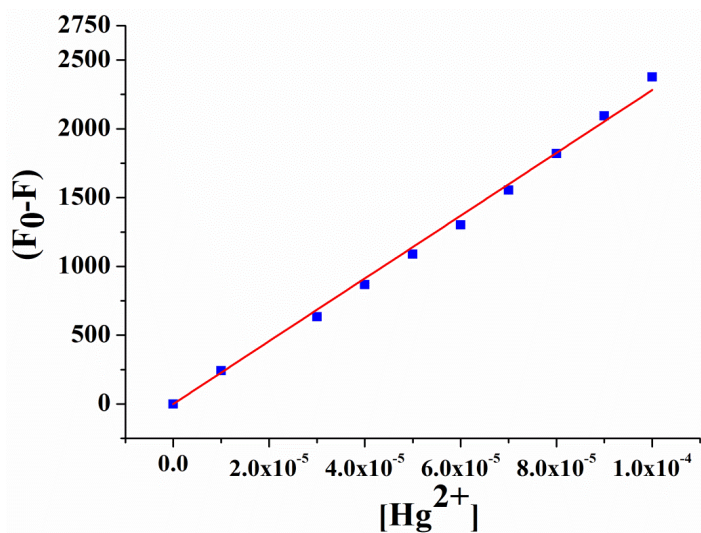


Fig. S26: Stern-Volmer plot for the quenching of **6** (red line) by incremental amount of Hg^{2+} .

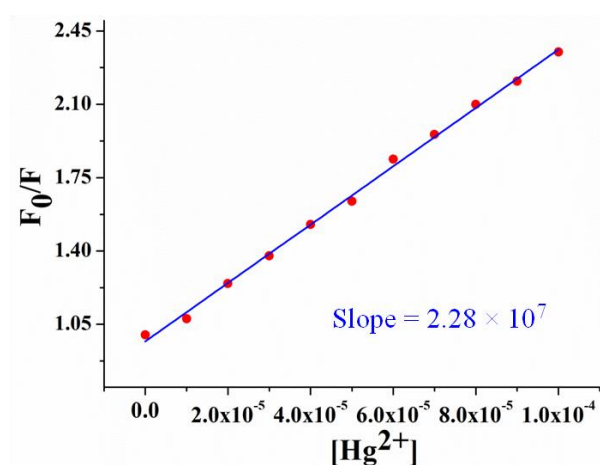


Fig. S27: The linear dynamic fluorescence response of **6** against Hg^{2+} to determine the limit of detection (LOD).

5g. Reversibility studies of **6**- Hg^{2+} by continuous variation of S^{2-} ion concentration

Reversibility studies were conducted by adding Hg^{2+} (1×10^{-5} M) to the **6** (1×10^{-5} M) solution followed by successive addition of S^{2-} (1×10^{-3} M).

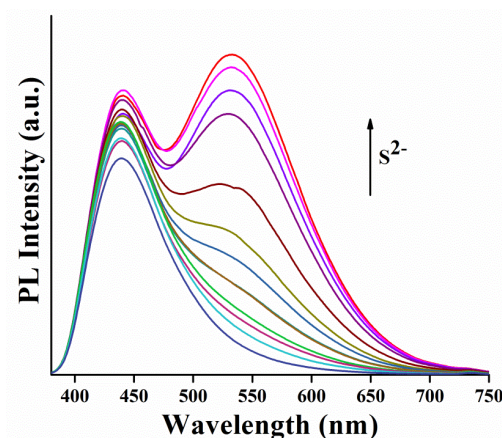


Fig S28: Fluorescence recovery responses of **6**- Hg^{2+} ($2\mu\text{M}$) upon successive addition of S^{2-} .

6. Theoretical studies

Computational Details: Theoretical calculations provide crucial insights to the experimental findings. In this study, all the theoretical calculations were performed with DFT^{S4,S5} and its time-dependent variant TDDFT,^{S6} as implemented in the Gaussian 16 programme package^{S7}. The ground state (S_0) geometries were optimized at the hybrid B3LYP/6-31G(D)^{S8} level of theory whereas the excited state (S_1) geometries were optimized at the range-separated hybrid CAM-B3LYP/6-31G(D)^{S9} level of theory. For the **6**- Hg^{2+} complex, a mixed basis set of Stuttgart/Dresden ECP (SDD) for Hg and 6-31G(D) for other atoms were used. The

weak dispersion interaction was accounted by introducing the Grimme's D3-dispersion correction with Becke-Johnson-damping function^{S10} (DFT-D3BJ). Second-order Hessian calculations were performed at each stationary points at the same computational level, to extract the thermochemical data as well as to authenticate the nature of the stationary points. The excitation energies were computed at the CAM-B3LYP/6-31+ G (D, P) level of theory which has been successfully used in the past for the charge-transfer systems^{S11,12} The solvation effects of the solvent chloroform ($\epsilon = 4.81$) and tetrahydrofuran ($\epsilon = 7.6$) were simulated by employing an explicit solvation model that uses the integral equation formalism (IEF) version^{S13} of the Polarizable Continuum Model (PCM)^{S14}, as implemented in Gaussian 16.

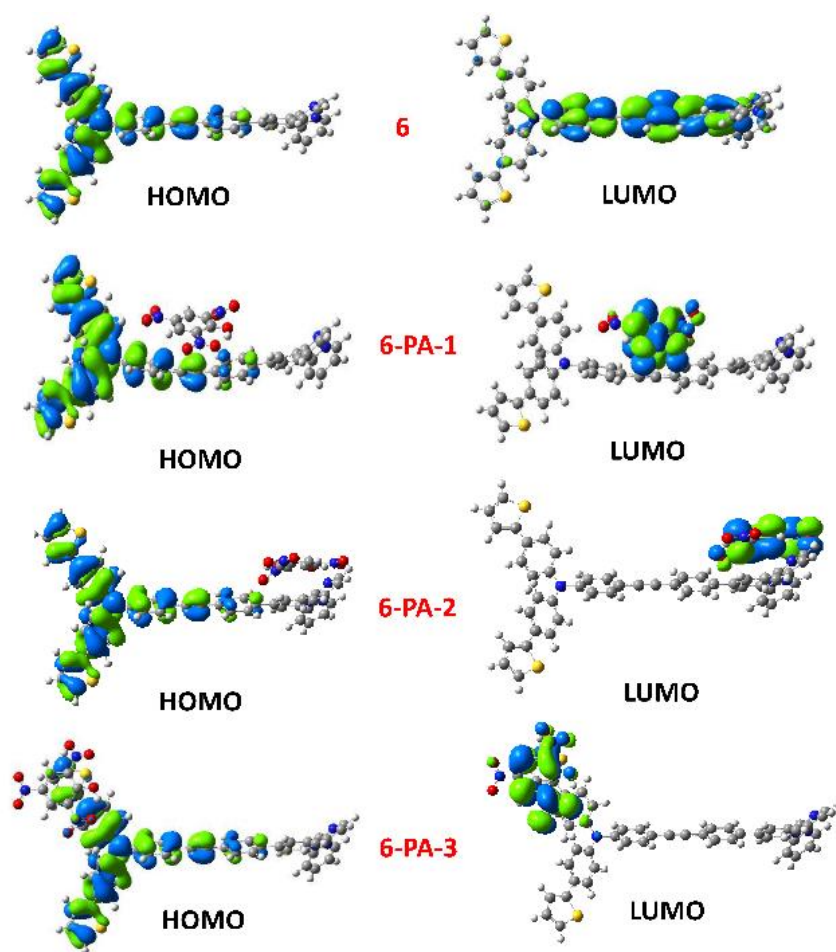


Fig. S29: Frontier molecular orbitals (FMO) of the probe **6** and three interaction complexes.

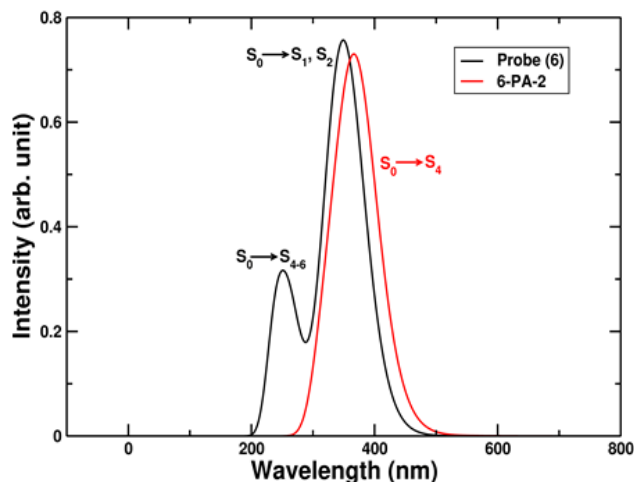


Fig. S30: Computed electronic spectra of the probe (**6**) and its complex with PA (**6-PA-2**).

Table S4: The detailed computed absorption and emission spectra data of probe **6** and its most stable complex with PA.

System	Transition	Wave length (nm)		Energy (eV)	f^a	Contrib ^b	CI ^c		
		Theoretical	Experimental						
6	Abs	$S_0 \rightarrow S_1$	358	366	3.46	2.08	H \rightarrow L	0.56	
		$S_0 \rightarrow S_2$	329		3.76	1.10	H \rightarrow L+1	0.65	
		$S_0 \rightarrow S_{4,6}$	288-265	280	4.30-4.69	0.15-0.33	Mixed Character		
	Em	$S_1 \rightarrow S_0$	435	507	3.04	2.25	L \rightarrow H	0.60	
6-PA-2	Abs	$S_0 \rightarrow S_1$	513		2.41	00	H \rightarrow L	0.68	
		$S_0 \rightarrow S_2$	398		3.11	0.02	H-7 \rightarrow L	0.18	
								H-10 \rightarrow L	0.15
		$S_0 \rightarrow S_3$	386		3.21	0.03	H-1 \rightarrow L	0.15	
		$S_0 \rightarrow S_4$	373		3.33	2.30	H4 \rightarrow L+1	0.12	
	Em	$S_1 \rightarrow S_0$	514	Quenched	2.41	0.002	L \rightarrow H	0.68	

^aOscillator strength, ^bH = HOMO and L = LUMO, ^cThe CI coefficients

Table S5: The Gibbs free energy data of different interaction products with respect to reactant.

	Gibbs free energy (a.u.)	Relative energy (kcal/mol)
6	-2901.45889	
PA	-920.922817	
6 + PA	-3822.38171	0
6-PA-1	-3822.39261	-06.83975
6-PA-2	-3822.40222	-12.87002
6-PA-3	-3822.39294	-07.04682

Table S6: The detailed computed absorption spectra of the probe **6** and **6-Hg²⁺** complex in THF.

System	Transition	Wave length (nm)		Energy (eV)	f ^a	Contributio n ^b	CI ^c	
		Theor etical	Experi mental					
6	Abs	S ₀ → S ₁	358	365	3.46	2.08	H → L	0.56
		S ₀ → S ₂	329	286	3.76	1.10	H -1 → L+1	0.14
6-Hg²⁺	Abs	S ₀ → S ₁	408	423	3.04	1.52	H → L	0.28
							H-1 → L+1	0.18
							H-1 → L +3.	0.10
		S ₀ → S ₄	325	338	3.82	0.42	H → L+1,L+3	0.37,0.45
		S ₀ → S ₅	298	290	4.15	0.22	H → L, L+1	0.28,0.57
S ₀ → S ₆	291		4.25	0.31	H-7 → L+1	0.5		

^aOscillator strength, ^bH = HOMO and L = LUMO, ^cCI coefficients

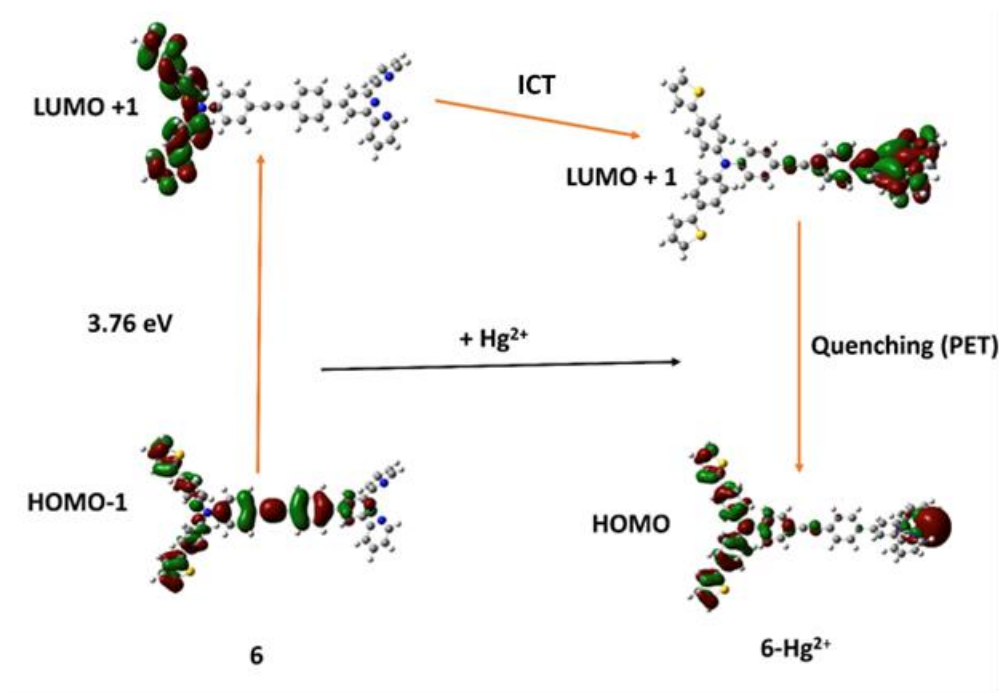


Fig. S31: Probable mechanism of change in fluorescence of probe **6** in presence of Hg^{2+} .

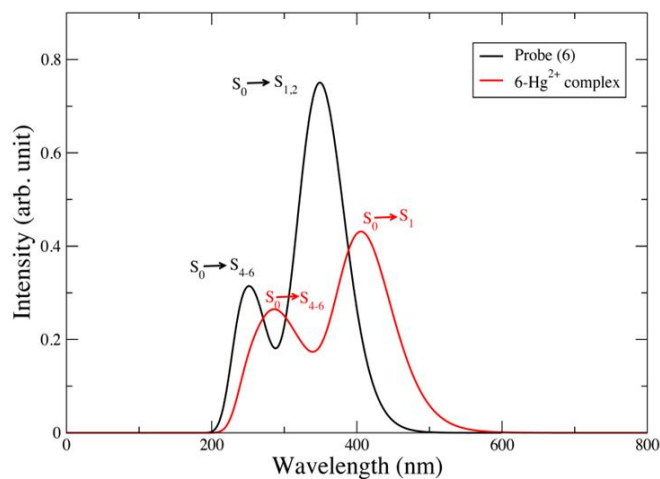


Fig. S32: Computed electronic spectra of the probe (**6**) and its complex with Hg^{2+} (**6-Hg²⁺**) in THF solvent.

7. References

- S1. (a) J. -F. Lefebvre, X. -Z. Sun, J. A. Calladine, M. W. George and E. A. Gibson, *Chem. Commun.*, 2014, **50**, 5258-5260. (b) A. Sil, D. Giri and S. K. Patra, *J. Mater. Chem. C*, 2017, **5**, 11100-11110
- S2. J. R. Lakowicz, *Principles of Fluorescence Spectroscopy*; Plenum: New York, 1999; Vol.

- S3. D. F. J. Arago, J. B. Biot, Mem. Acad. Fr. 1806, 7.
- S4. Kohn, W.; Sham, L. J. Self-Consistent Equations Including Exchange and Correlation Effects. *Phys. Rev.* **1965**, *140*, A1133.
- S5. Kohn, W.; Becke, A. D.; Parr, R. G. Density Functional Theory of Electronic Structure. *J. Phys. Chem.* **1996**, *100*, 12974–12980.
- S6. Bauernschmitt, R.; Ahlrichs, R. Treatment of Electronic Excitations within the Adiabatic Approximation of Time Dependent Density Functional Theory. *Chem. Phys. Lett.* **1996**, *256*, 454–464.
- S7. Gaussian09, R. A. 1, Mj Frisch, Gw Trucks, Hb Schlegel, Ge Scuseria, Ma Robb, Jr Cheeseman, g. Scalmani, v. Barone, b. Mennucci, Ga Petersson et Al., Gaussian. Inc., Wallingford CT **2009**, *121*, 150–166.
- S8. Stephens, P. J.; Devlin, F. J.; Chabalowski, C. F.; Frisch, M. J. Ab Initio Calculation of Vibrational Absorption and Circular Dichroism Spectra Using Density Functional Force Fields. *J. Phys. Chem.* **1994**, *98*, 11623–11627.
- S9. Yanai, T.; Tew, D. P.; Handy, N. C. A New Hybrid Exchange–Correlation Functional Using the Coulomb–Attenuating Method (CAM-B3LYP). *Chem. Phys. Lett.* **2004**, *393*, 51–57.
- S10. Grimme, S.; Antony, J.; Ehrlich, S.; Krieg, H. A Consistent and Accurate Ab Initio Parametrization of Density Functional Dispersion Correction (DFT-D) for the 94 Elements H–Pu. *J. Chem. Phys.* **2010**, *132*, 154104.
- S11. Zhou, P.; Liu, J.; Yang, S.; Chen, J.; Han, K.; He, G. The Invalidity of the Photo-Induced Electron Transfer Mechanism for Fluorescein Derivatives. *Phys. Chem. Chem. Phys.* **2012**, *14*, 15191–15198.
- S12. Lu, M.; Zhou, P.; Ma, Y.; Tang, Z.; Yang, Y.; Han, K. Reconsideration of the Detection and Fluorescence Mechanism of a Pyrene-Based Chemosensor for TNT. *J. Phys. Chem. A* **2018**, *122*, 1400–1405.
- S13. Cancès, E.; Mennucci, B.; Tomasi, J. A New Integral Equation Formalism for the Polarizable Continuum Model: Theoretical Background and Applications to Isotropic and Anisotropic Dielectrics. *J. Chem. Phys.* **1997**, *107*, 3032–3041.
- S14. Miertuš, S.; Scrocco, E.; Tomasi, J. Electrostatic Interaction of a Solute with a Continuum. A Direct Utilizaion of AB Initio Molecular Potentials for the Prevision of Solvent Effects. *Chem. Phys.* **1981**, *55*, 117–129.